UNCLASSIFIED

AD **263 478**

Reproduced
by the

ARMED SERVICES TECHNICAL INFORMATION AGENCY
ARLINGTON HALL STATION
ARLINGTON 12, VIRGINIA
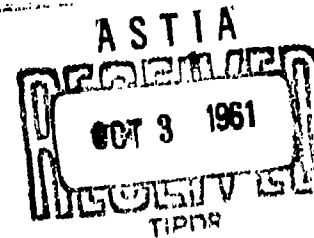
DOPPLER SPECTRAL CHARACTERISTICS
OF AIRCRAFT RADAR TARGETS AT S-BAND

R. E. Gardner

Equipment Research Branch
Radar Division

August 3, 1961

CONTENTS

ABSTRACT

The doppler frequency spectra of propeller-driven and turbojet aircraft have been measured at S-band. It was found that there are numerous spectral lines in the doppler return from propeller-driven aircraft resulting form the relative motion of the propellers with respect to the radar. The doppler spectrum can be roughly predicted from a knowledge of the propeller parameters and target aspect. Turbojet aircraft spectra were found to contain a strong modulation sideband due to the engine compressor blades. Doppler velocity noise due to target scintillation was also measured.

PROBLEM STATUS

DOPPLER SPECTRAL CHARACTERISTICS
OF AIRCRAFT RADAR TARGETS AT S-BAND

INTRODUCTION

Doppler radar detects targets by virtue of their velocity with respect to the transmitter antenna. If the target is a small rigid body with only pure translational motion, the received signal after being compared to the transmitted signal will consist of only a single spectral line at a frequency of $f_d = 2v/\lambda$, where v is the radial velocity of the target and λ is the transmitted wavelength. This doppler information is usually processed by first passing it through filters of various descriptions such as single wide-band filters covering the desired doppler frequency range, single narrow-band electronically tuned filters, or banks of contiguously tuned narrow-band filters. The purpose of the filters, depending upon the application of the radar, might be to exclude stationary targets or clutter, resolve multiple targets with different velocities, or to enhance signal-to-noise ratio.

An aircraft target, however, has not only finite size and rotational motion, but also moving parts such as propellers or compressor and turbine blades. Because a target has finite size and irregular geometry it presents a distribution of reflecting surfaces over the extent of the target. In flight the target will roll, pitch, yaw, and vibrate, causing changes in intensity and position of these reflecting surfaces with time, about an average value. Since the received echo is the vector sum of the individual echos from these reflecting surfaces, the resultant echo will also change with time about an average value. This phenomenon is well known and results in what is known as angle, range, and amplitude noise in conventional pulse tracking radars. In pulse doppler radars, however, it results also in velocity noise, which has the effect of broadening the doppler spectrum line to a finite width depending upon the frequency deviation and spectral distribution of the noise. This imposes a limit as to how narrow a bandwidth may be used for the doppler filters, thus limiting, for example, the accuracy to which a target's velocity can be determined.

The motion of an aircraft target's propellers, in addition to causing some amplitude modulation of the airframe doppler signal, produces doppler signals of its own. Since the return from a propeller is periodic at the blade rotational frequency, and the blade tip velocity approaches Mach 1.0, the spectrum of the propeller doppler signal at most aspect angles is quite complex and is separate and distinct from that of the airframe doppler signal. In some doppler radar systems this propeller return may appear as spurious signals causing false target detections.

In the case of turbojet aircraft, modulation is produced by the compressor or turbine blades of the engine. Even though the engines are usually totally enclosed, except for intake and exhaust ducts sometimes 16 ft in length, there is sufficient propagation down the ducts at microwave frequencies to allow ample amounts of rf energy to be modulated by the blades. Since compressors and turbines contain relatively large numbers of blades rotating at high angular frequencies, the modulation frequencies will be much higher than those of propeller driven aircraft (usually above 1000 cps). The modulation sidebands produced by the blades are easily distinguished and, depending upon aspect angle and transmitter frequency, can be quite strong compared to the airframe doppler return. Thus, a modulation sideband can be quite easily mistaken for a separate target with a different velocity.

THE PULSE DOPPLER RADAR

The system used in this investigation consists of a coherent pulse doppler radar on an S-band frequency of 2830 Mc, giving a doppler frequency of 9.7 cps/knot. Figure 1 shows a simplified block diagram of the system. The stalo, or stable local oscillator, is an actively stabilized reflex klystron cw oscillator operating on a frequency of 2800 Mc. Its output is used both as drive for the synchrodyne and local oscillator injection for microwave mixer. The synchrodyne is a 3-cavity klystron phase-modulated at 30 Mc to produce an output at 2800 Mc which drives the power amplifier. The power amplifier is a 3-cavity klystron modulated with a 1.0-μs pulse at a prf of 12 kc and has a peak output power of 7 kw. The receiver i-f output is fed to a phase detector whose reference is the same 30 Mc used to modulate the synchrodyne.
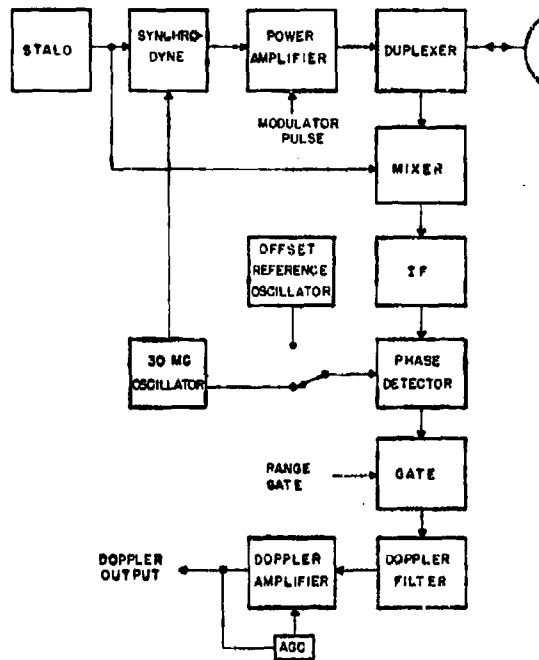

Fig. 1 - Simplified block diagram of the
pulse doppler radar system

The received signal is actually a pulse spectrum that has been shifted in frequency by an amount of f_d as shown in Fig. 2(a). Figure 2(b) shows the spectrum at the phase detector output after being folded about the center spectrum line. The doppler filter passband is placed adjacent to the center spectrum line, and in this case, covers the range of frequencies from 100 cps to 6000 cps, corresponding to velocities from approximately 10 to 600 knots, thereby excluding stationary targets and clutter with velocities up to 10 knots. Because of folding, both approaching and receding targets appear in the filter passband and cannot be distinguished.
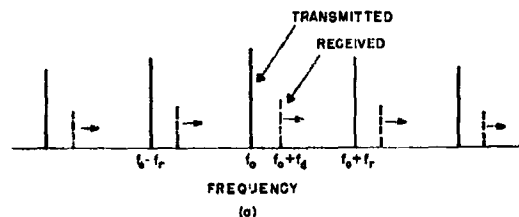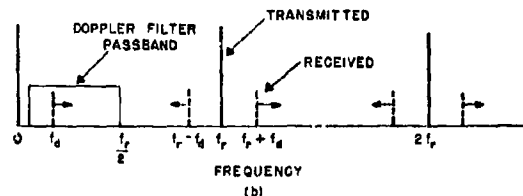
Fig. 2 - (a) Transmitted and received pulse spectrum of an approaching target with increasing doppler frequency; (b) spectrum at phase detector output after being folded about zero frequency

In order to measure the doppler spectrum around zero velocity, or to be able to determine the sense of direction of velocity, the phase detector reference can be offset from 30 Mc by the desired amount by using a separate oscillator for the reference. An offset will appear to shift the doppler frequency spectrum by the amount of the offset.

Actually, this radar has two prf's and is capable of automatically tracking targets in range, angle, and velocity. However, the only factor that affects the application of the data presented in this report to other doppler radars (either pulse or cw) is the transmitter frequency.

OVERALL DOPPLER FREQUENCY SPECTRUM

Measurement Technique

All of the aircraft used as targets for this investigation, with one exception, were targets of opportunity. However, the close proximity of one commercial and two military airfields gave access to an almost unlimited variety of aircraft and flight configurations to be used as radar targets. Over the past three years much data have been collected and analyzed as a by-product of a program of investigation of pulse doppler radar techniques, but of course only a small representative portion of it is presented here.

The doppler frequencies at S-band of most available targets fall in the audio spectrum, and thus can be easily recorded on magnetic tape for later analysis.

The technique used to obtain the doppler frequency spectra of targets was first to continuously record the signal on tape at any convenient tape speed. Later, a section of the recording for which analysis is desired is re-recorded at a high tape speed, 30 ips, for example. The re-recorded tape is then spliced into a continuous 39-in. loop and played back at 7.5 ips. This takes a 1.3-second sample of the original signal and repeats it every 5.2 seconds at 1/4 the original frequency. The loop playback output is fed into a Panoramic Radio Products Model LF-2aM Spectrum Analyzer, which prints out a continuous chart recording of the spectrum of any 20-, 100-, or 500-cps interval in the frequency range 0-2500 cps. Since the original signal frequency spectrum is divided by four by tape speed reduction, the 0-500-cps interval of analyzer output will represent 0-2000 cps in real

frequency. Some integration was added to smooth the data over a full revolution of the tape loop. A variety of analyzer bandwidths and sweep speeds are available so that the combination commensurate with the resolution and integration time desired may be selected. For example, with a 5.2-second loop playback period, the analyzer bandwidth was set at 2.7 cps with a sweep rate of 500 cps analyzer frequency per 12 min.

Propeller-Driven Aircraft

A typical doppler frequency spectrum of a propeller-driven aircraft, a DC-7 in this example, is shown in Fig. 3. The most prevalent spectral line, of course, is the doppler return from the airframe, denoting its radial velocity. Some amplitude modulation side-bands at the propeller blade frequency appear around the airframe line. This amplitude modulation can be caused by the propeller blade chopping a portion of the reflected radar energy from the airframe, thereby periodically modulating the received echo.
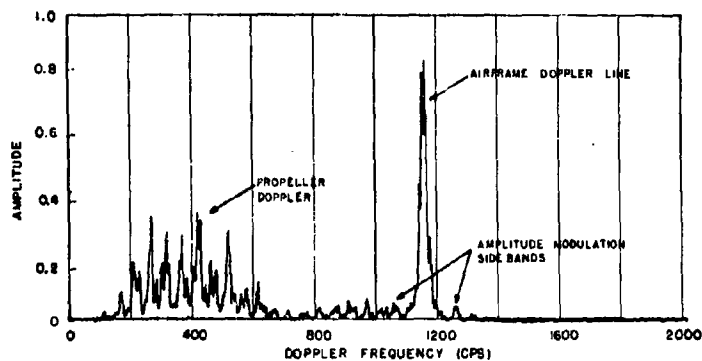

Fig. 3 - A typical doppler frequency spectrum of a
propeller-driven aircraft

Another group of spectral lines can be found at a lower frequency than the airframe line. These are the result of reflected energy from the rotating propeller blades themselves, thus creating doppler frequencies proportional to the vector sum of the radial components of the airframe velocity and the propeller tangential velocity at the radius of the reflecting surface. Since a propeller has a varying blade angle along its length, the position of the reflecting area on the blade depends upon the viewing angle and blade angular position. Thus, the propeller doppler return is modulated at the blade frequency, and the center frequency of its spectrum is dependent upon aspect angle. Figure 4 shows the doppler spectrum due to the rotating propellers alone of an aircraft sitting on a runway, the airframe line having been removed by the doppler filter at zero frequency.

In a system that folds the spectrum about zero, the major portion of the propeller doppler spectrum will always be lower in frequency than the airframe line because the pitch angle of propeller blades is in such a direction that the blade with the largest reflecting area toward the radar has its radial component of velocity in a direction opposite to that of the airframe regardless of aircraft direction of flight relative to the radar. The following detailed discussion will consider the two cases of a receding and an approaching target.
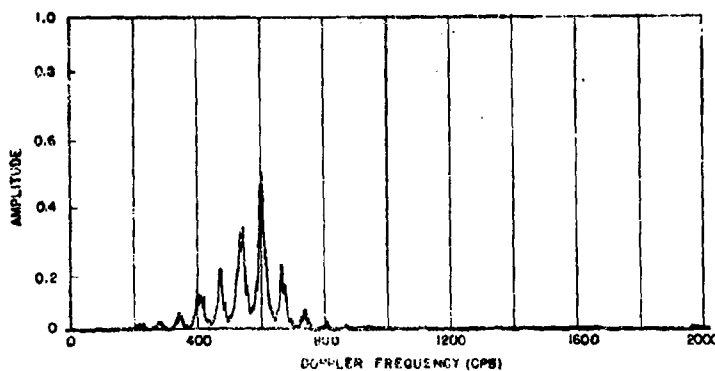
Fig. 4 - Doppler spectrum due to rotating propellers
on a stationary aircraft

First, consider the case of a receding target. A cross section of an element of a propeller blade has the shape of an airfoil. Along the outer two-thirds radius of the propeller blade the rear side is relatively flat. Toward the propeller root, the airfoil is modified for structural purposes and is more rounded. The blade angle, defined as the angle between the plane of rotation and the chord of the blade element cross section, varies from a small angle at the tip to larger angles toward the root. A typical blade may have angles from 15^0 at the tip to 30^0 at one-third radius. Maximum reflection will occur when a flat surface element is perpendicular to the radar line of sight. This occurs at a radius where the blade angle equals the aspect with respect to the propeller axis.

To aid visualizing this maximum reflection point, a model airplane propeller having nearly the same proportions as a full-sized propeller was utilized. While the propeller was being rotated by a motor, a point source of light simulating the radar transmitter was directed at it at various angles with respect to the axis of rotation. A slide projector was used as the light source and a camera near the same position was used to photograph the resulting specular reflection from the element of blade surface perpendicular to it. Similar optical methods have been used to estimate the radar cross section of aircraft and determine the locations of specular reflection using a highly polished aircraft model (1). Figure 5 shows this reflection from the rear side of the propeller at angles with respect to the propeller axis from 15^0 to 30^0, corresponding to the blade angle at the tip and one-third radius, respectively.
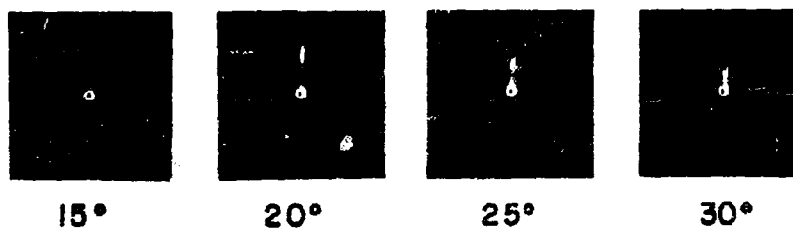

15°   20°   25°   30°

Fig. 5 - Optical reflection from the rear of a model airplane propeller with the line of sight at various angles from the propeller axis

Actually, the reflected beamwidth will appear somewhat larger at S-band with a full-size propeller than indicated in Fig. 5. A flat conducting surface of area A whose dimensions are large compared to a wavelength will have a radar cross section of

$$\sigma = \frac{4\pi A^2}{\lambda^2}.$$

The reflected energy will be in the form of a lobe structure with the main lobe approximately λ/a radians wide, where a is some suitably determined average dimension of the flat plate. Excluding the main lobe, at a small angle θ from the normal, the radar cross section averaged over several lobes is approximately

$$\sigma \approx \frac{4\pi \lambda^2}{(2\pi \theta)^2}$$

From these relationships (2,3) it can be seen that the smaller the dimensions of the reflecting surface and the longer the wavelength, the wider will be the pattern of the reflected energy as a function of θ.

When the dimensions of the reflecting surface are comparable to a wavelength, these relationships no longer exactly hold; in general the radar cross section will be reduced and the lobe pattern will be altered. Because of a propeller blade's complex geometry, no exact analysis was made of its reflection characteristics beyond the scope of the above relationships. The width of experimentally observed propeller blade reflection patterns of receding targets at various aspects averaged from about 22.5^0 to 45^0 out of a complete 360^0 blade revolution.

A vector diagram of the velocity components of a propeller blade element which is perpendicular to the radar line of sight is shown in Fig. 6, in which β is the aspect angle with respect to the propeller axis of rotation (or aircraft line of flight) and is also the blade angle at the radius of the element, v_a is the airframe velocity, ωr is the tangential velocity of the blade at the radius r of the element, V_p is the resultant total velocity of the element, and V_{a_r} and V_{p_r} are the radial components of V_a and V_p in the direction of the radar from which the doppler frequencies are derived.
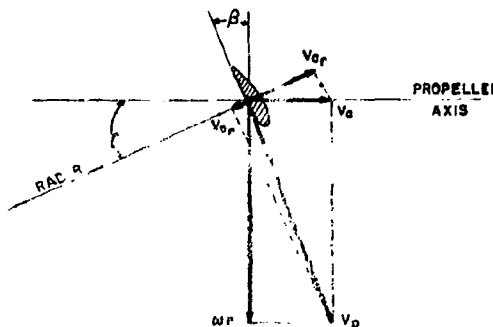

Fig. 6 - Vector diagram of the velocity components of a propeller blade element of a receding aircraft

For example, assume a single-engine target aircraft with the following characteristics:

speed	135 knots
propeller blades	4
propeller speed	1125 rpm
aspect angle	20^0
radius at 20-degree blade angle	6.0 ft.

Now, V_a = 228 ft/sec, ωr = $(2\pi)(1125/60)(6)$ = 706 ft/sec, and V_p = 742 ft/sec. The radial components of V_a and V_p will be V_{a_r} = -214 ft/sec and V_{p_r} = 27.2 ft/sec. The doppler frequencies corresponding to these velocities are 1230 cps and 156 cps respectively. However, the doppler return due to V_{p_r} will not be constant in amplitude with time, but will be chopped at the blade frequency of (1125/60)(4) = 75 cps. If it is assumed the blade reflecting element has a reflection pattern 22.5^0 wide, then with 4 blades the duty cycle of the received doppler signal from the propeller will be (22.5/360)(4) = 0.25. Assuming, for simplicity, a rectangular pulse, the doppler spectrum of the propeller return consists of lines 75 cps apart with a sin x/x amplitude distribution about a center frequency of 156 cps and the first zeros 600 cps apart. Figure 7 shows the composite doppler spectrum of this example of a receding target with receding velocities to the right of zero and closing velocities to the left. Unless the phase detector reference frequency is offset, the actual spectrum would be folded about zero so that all of the spectrum would appear to the right of zero. Of course, an actual spectrum will not appear exactly identical to this hypothetical example, but it does show the general trend.

Fig. 7 - Doppler spectrum of a
hypothetical receding single-
engine propeller-driven aircraft

DOPPLER FREQUENCY (cps)
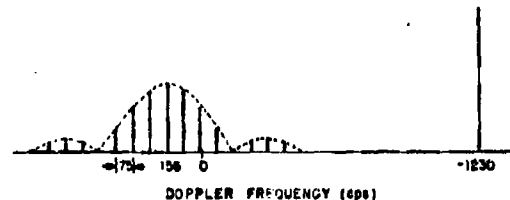
In the case of the multiengine aircraft, the propeller doppler spectrum will not appear greatly different, because the propeller speeds are always closely synchronized with each other so that the spectrum lines resulting from each of the propellers will fall at the same frequencies. However, the sin x/x amplitude distribution may be altered somewhat. If the propellers do not have the same angular alignment, the doppler signal will be in the form of pairs or groups of pulses with the same basic propeller blade frequency. A Fourier analysis of a rectangular pulse-pair train is given in Appendix A.

Figure 8 shows a series of actual doppler spectra of a receding two-engine aircraft at various aspect angles. The angles were computed using the range, azimuth, and elevation of the target at intervals during a passing course, assuming no drift. Although the phase detector reference oscillator was offset 800 cps in such a direction from the zero-velocity i-f frequency of 30 Mc that zero velocity appeared at 800 cps with receding velocities appearing higher in frequency, the charts are labeled in true doppler frequency; i.e., zero doppler on the frequency scale actually falls at 800 cps analyzer output. The amplitude scale is approximately logarithmic and is calibrated in db, thereby allowing some of the lower amplitude spectrum lines to be seen more easily. Note that the propeller doppler pulse spectrum is most clearly defined between the aspect angles of 15^0 and 37^0,

corresponding to the blade angles for which strong specular reflection can be obtained. Since the pitch of most propellers can be changed or is automatically changed, the aspects for which strong specular reflections are obtained will be a function also of pitch setting. There are some doppler returns from the propellers at almost all other angles, possibly due to reflections from the edges of the blades or rounded sections toward the root. However, these returns are generally somewhat weaker and are almost nonexistent at an aspect of 90°. There is also the possibility of multiple reflections between the propeller and airframe.

A time picture of typical propeller doppler returns from a single-engine AD-5 and a four-engine DC-7 are shown in Fig. 9. These plots were obtained by filtering the airframe doppler line from the playback output of a section of the tape recording, leaving only the propeller doppler. The width of the trace is 10 cm and the time scale is 5 ms/cm for the AD-5 and 10 ms/cm for the DC-7. Note that the AD-5 propeller return consists of distinct pulses of a doppler carrier at a repetition frequency of 75 cps, while the combined return from the four propellers of the DC-7 appears quite complex.

Now consider an approaching target. The reflection as a function of blade position from the front of a propeller is not quite so simple because of the curvature of the blade due to the airfoil shape. Again, the model propeller and light source are helpful in visualizing the characteristic of the reflection. Figure 10 shows the stationary model propeller at aspect angles of 0°, 30°, and 60°. Figure 11 shows the optical reflections from the front of the propeller at aspect angles from 0° to 60°. Note that now, instead of a single reflection point as was the case for the rear side, the point of maximum reflection changes radius as a function of the blade angular position.

In the upper half of the pattern the blade is receding from the observer. At small aspect angles, less than about 10°, the strength of the reflection from the approaching half of the pattern appears almost equal to that from the receding half and would cause some propeller doppler return higher in frequency than the airframe line. However, at larger aspect angles it can be seen that the predominant return is from the receding blades, as was the case for the rear side of the propeller.

Again, the radar reflection pattern will be somewhat wider than the optical reflections because of the blade's dimensions compared to a wavelength. Except for the edges, the radii of curvature of the airfoil contour of the front of a propeller blade are usually greater than a wavelength at S-band, so that considerable radar return is possible. (If the radius of curvature is very small compared to a wavelength, the radar return approximates Rayleigh's scattering law and is very dependent upon polarization.)

Figure 12 is a vector diagram of the various velocity components of a blade's reflecting element. As shown, θ is the angular position of the blade, r is the radius of the reflecting element on a blade of radius R, and β is the aspect angle between the propeller axis and the radar line of sight. Because of the curvature of the surface, maximum reflection can occur when the blade radius is at angles other than a right angle to the line of sight. This makes it necessary to show the various components in two planes; first in the plane of rotation, then in the plane common to the axis of rotation and the radar. For simplicity of illustration it is assumed that the axis of rotation and the radar lie in a common horizontal plane. The radial component of velocity of the reflecting element with respect to the airframe is seen to be

$$V_r = \omega r \sin \theta \sin \beta.$$

This must be vectorially added to the airframe radial velocity in order to obtain the resultant total reflecting element radial velocity.
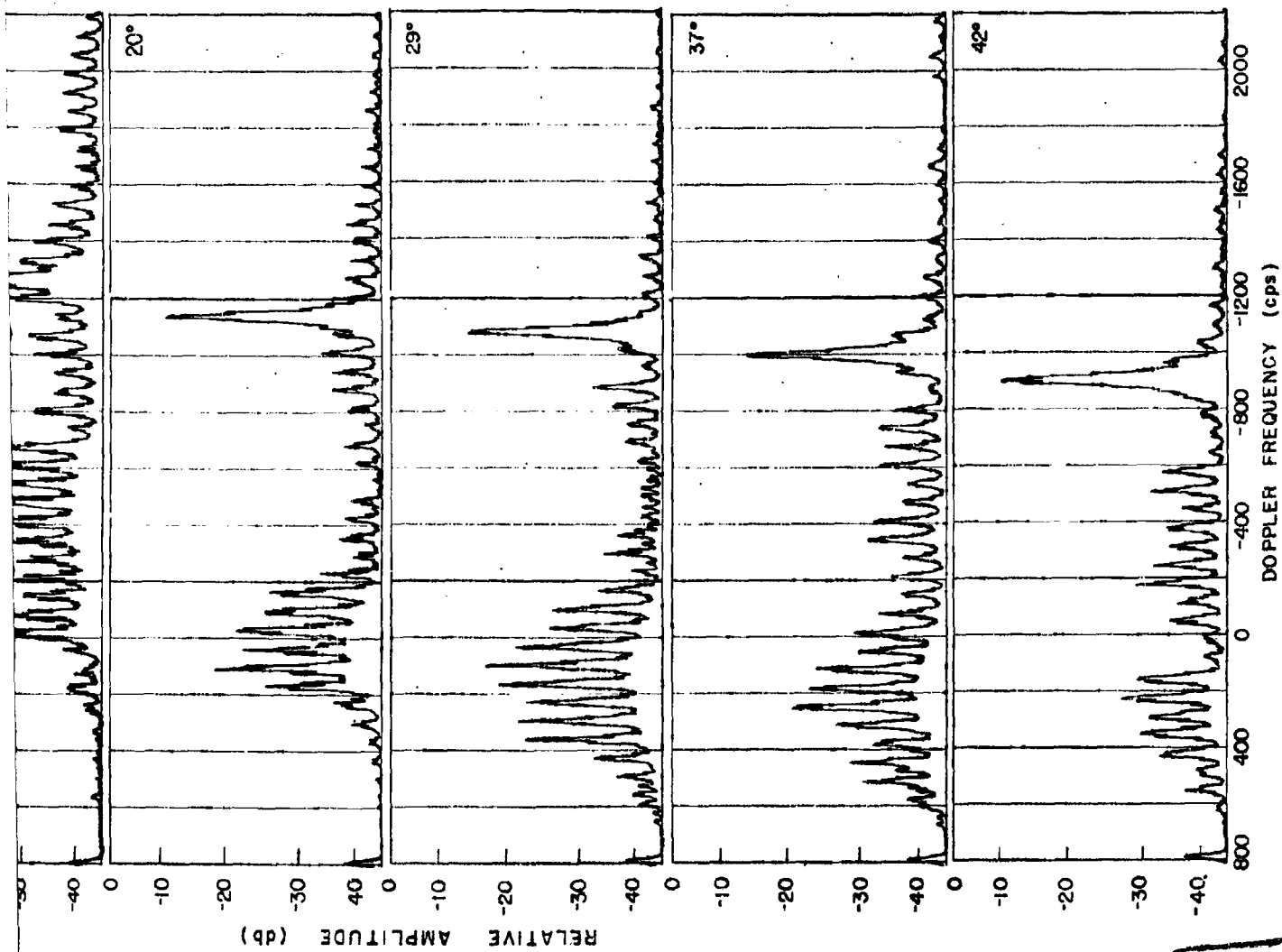
RELATIVE AMPLITUDE (db)
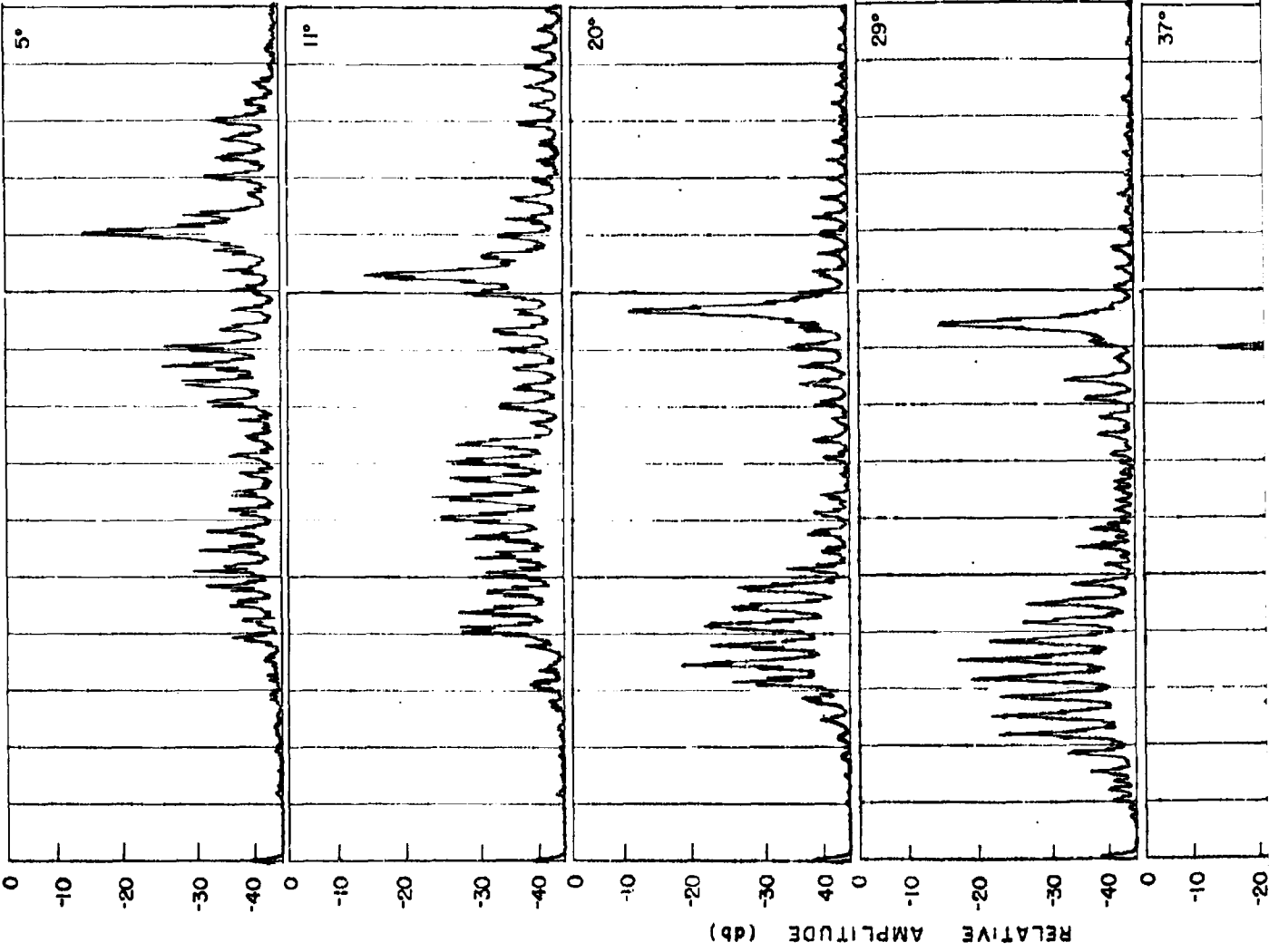
Fig. 8 – Doppler spectra of a receding two-engine propeller-driven aircraft
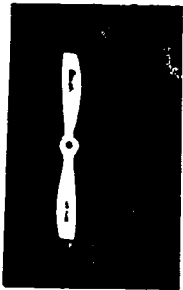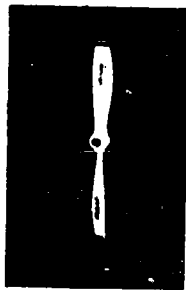
(a)

Fig. 9 - Time-amplitude pic-
tures of the propeller doppler
return of (a) an AD-5 and (b)
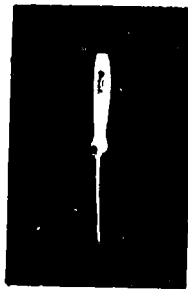a DC-7

(b)

0°   30°   60°

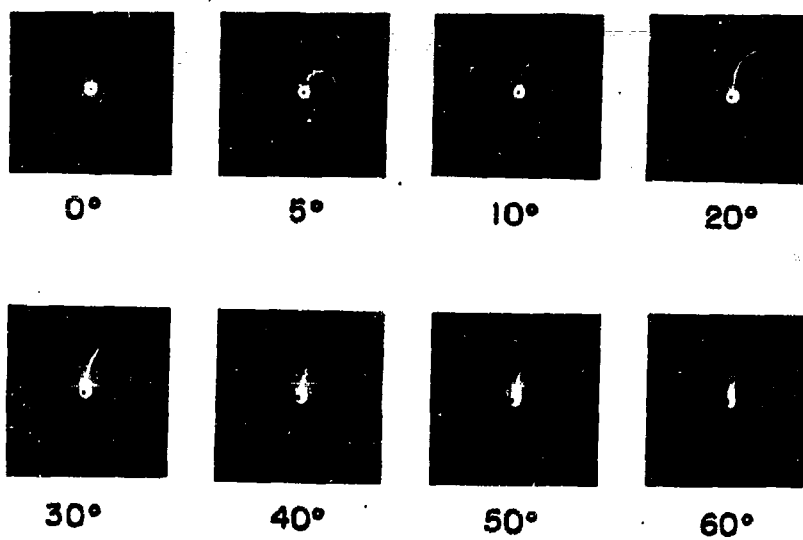Fig. 10 - View of a stationary model
airplane propeller

Fig. 11 - Optical reflection from the front of the
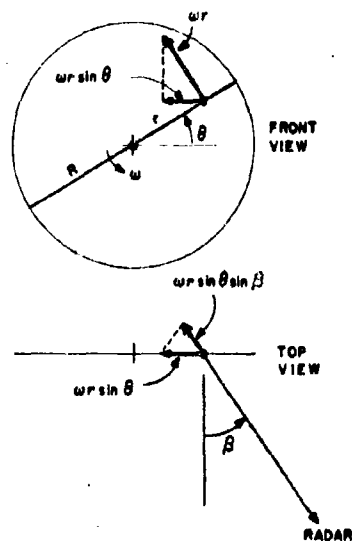model airplane propeller of Fig. 10

Fig. 12 - Velocity components
of a propeller blade element

As an example, at an aspect angle β of 10^0, assume the reflecting element follows a circular path similar to that shown in the photograph of Fig. 10. Figure 13 is a schematic approximation of the path. The radius of the reflecting element, r, as a function of θ is approximated by

$$r = 0.9 R \cos \theta, \qquad 270° < \theta < 90°.$$

The radial velocity of the element will then be

$$V_r = 0.9 \omega R \sin \beta \cos \theta \sin \theta$$

$$= \frac{0.9 \omega R}{2} \sin \beta \sin 2\theta, \qquad 270° < \theta < 90°.$$

Since $\theta = \omega t$ and $\sin \beta = 0.174$ for $\beta = 10^0$,

$$V_r = 0.078 \omega R \sin 2\omega t.$$

Fig. 13 - Approximate path of the assumed reflecting element on the front of a propeller for aspects of 10^0 and 30^0
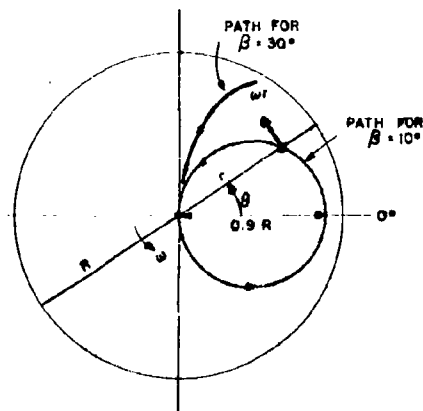
If this is a two-bladed propeller, the pattern will be repeated every 180^0 of rotation, and V_r therefore will be a continuous sinusoidal function with a frequency of $2\omega t$ and a maximum value of $0.078 \omega R$. Figure 14 is a plot of the radial velocity with respect to the airframe normalized to ωR of the reflecting element as a function of time.

Figure 14 also shows a second example: an aspect angle of 30^0. The reflecting element, as indicated by the photographs, exists now only between the angles of 60^0 and 85^0 and follows the approximate path included in Fig. 13. The radial velocity of the point as a function of time was plotted in Fig. 14 using values obtained by measuring r and θ along the path. The maximum radial velocity occurs at $\theta = 60^0$ and is equal to $0.41 \omega R$. Again, assuming a two-bladed propeller, this pattern will be repeated every 180^0. In general, if n is the number of propeller blades, the modulation frequency will be $n\omega t$, corresponding to the blade frequency.

The signal return from the front of a rotating propeller blade, such as that resulting from the conditions of the above example, contains a combination of frequency and amplitude
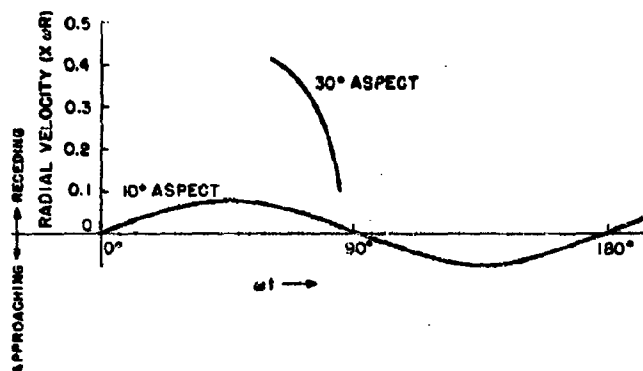
Fig. 14 - Radial velocity, as a function of time, of the reflecting element on the front of a 2-bladed propeller relative to the airframe for aspects of 10^0 and 30^0, normalized to the blade tip tangential velocity

modulation of complex waveforms, so that only the approximate envelope of its doppler frequency spectrum can be obtained without undue difficulty. Since both the basic FM and AM modulating frequencies are the same, the spectrum will contain only lines spaced by the modulation frequency. The band of frequencies encompassing all the spectrum lines of significant amplitude is given approximately by

$$\Delta F = \Delta f_{p-p} + 2 f_m$$

where Δf_{p-p} is the peak to peak frequency deviation, and f_m is the highest frequency component of significant amplitude of the modulating waveform.

The approximate doppler spectra resulting from the waveforms of the two examples in Fig. 14 will now be computed. Assume an approaching aircraft with the following characteristics:

airspeed	120 knots
propeller radius	3.32 ft
number of blades	2
propeller speed	2400 rpm.

The tangential velocity of the blade tip is $\omega R = (2\pi)(2400/60)(3.32) = 834$ ft/sec and the modulation frequency is $(2400/60)(2) = 80$ cps. At an aspect of 10^0 the maximum radial velocity of the reflecting element is $0.078 \, \omega R = 65$ ft/sec relative to the airframe. The airframe radial velocity is $120 \cos 10^0 = 118$ knots. Assuming that the amplitude of the radar return from the propeller when the blade is approaching averages one-half the amplitude when it is receding relative to the airframe, the approximate doppler frequency spectrum will appear as indicated in Fig. 15(a). The peak deviation here is 65 ft/sec, or a doppler frequency of 374 cps. Because the assumed circular path of the reflecting element resulted in sinusoidal frequency modulation in this example, the spectrum can be found by conventional methods using a modulation index of $374/80 = 4.8$. However, the spectrum amplitude distribution will be assymetrical because of the assumed characteristic of the amplitude modulation.
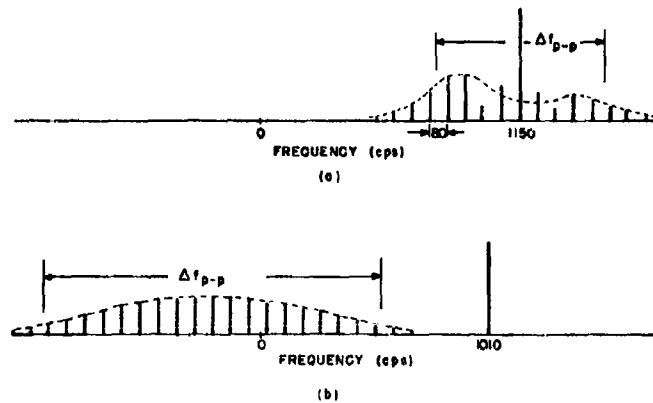
Fig. 15 - Doppler frequency spectra of
a hypothetical approaching target at
aspects of (a) 10° and (b) 30°

At an aspect of 30°, the maximum radial velocity of the reflecting element is 0.41 ωR = 340 ft/sec, or 1960 cps, relative to the airframe, while the minimum is 0.1 ωR = 83 ft/sec, or 480 cps. Note that these velocities are receding relative to the airframe. This gives a peak-to-peak deviation of 1480 cps, resulting in a propeller doppler spectrum only slightly wider than this. Assuming also an amplitude modulation characteristic such that the radar return is a maximum when r = 0.5 R, the average amplitude of the propeller doppler spectrum envelope will peak at the approximate center, and the overall spectrum might appear as in Fig. 15(b).

It should be emphasized again that these hypothetical examples are to be taken merely as guides to explain the mechanism of production of propeller doppler spectra. The values used were arbitrarily chosen for convenience, but they do happen to be the approximate parameters of particular aircraft. Actually, the doppler spectrum is approximately the same regardless of aircraft type because propeller design is more or less standardized. The blade tip speed, ωR, is always less than sonic speed and usually in the vicinity of 800 ft/sec, and the blade frequency is usually between 50 and 90 cps.

Figure 16 is a series of doppler spectra of an approaching two-engine aircraft at various aspect angles. In obtaining these spectra the phase detector was again offset 800 cps, but this time in such a direction that approaching velocities appear at an output higher than 800 cps. Note that at small aspect angles the propeller doppler spectrum is confined mostly to the region around the airframe line, and that at larger angles it has a much wider spread into the region lower in frequency than the airframe line. At aspects larger than about 40°, the relative amplitude of the propeller doppler spectrum lines is much reduced. It is difficult to distinguish the amplitude modulation sidebands resulting from the propellers chopping part of the airframe echo at small aspect angles when the propeller doppler spectrum is also concentrated in the region around the airframe line, but at larger aspects where the propeller doppler spectrum spreads into the lower frequency region, some amplitude modulation sidebands can be seen around the airframe line. Note the particularly strong pair of amplitude modulation sidebands around the airframe line in the spectrum at the 13° aspect.

Figure 17 shows time pictures of the propeller doppler signal from the above target. Some frequency modulation can be seen in the return for the 26° aspect. At an 18° aspect,

the return exists for a greater part of a propeller revolution, but the frequency deviation is not great enough to be readily apparent in the photographs as frequency modulation.

The preceding examples of both receding and approaching propeller-driven aircraft were taken either shortly after take-off or shortly before landing, as these were the targets most often available. Under these flight situations, the propeller pitch is usually set to a small angle, and the aircraft speed is relatively low. Under cruising conditions, however, the propeller pitch is greater, and of course the aircraft speed is higher. The propeller speed usually remains essentially constant, but may be slightly higher during take-off and landing. Thus, the doppler spectrum also depends, to some extent, upon the flight phase. The spectrum of a cruising aircraft will not appear greatly different from the preceding examples, except that the aspect for which a given propeller doppler spectral amplitude distribution is obtained will be slightly different.

Turbojet Aircraft

Considerable modulation is produced by the compressor blades of turbojet engines. The dimensions of the air intake ducts are very large compared to a wavelength at S-band, so that radar energy is very easily propagated down them to the compressor stages and back. Since the duct's dimensions are so large, it probably acts as a waveguide which is far above cut-off frequency and is terminated by the compressor, thus making the reflected energy a function of changes in the termination such as would be produced by the rotating compressor blades. The first-stage compressor blades of some engines are about two wavelengths long at S-band. Modulation of the rf energy produced by the rotating blades would contain both phase and amplitude modulation at the blade frequency. It is known that these air ducts produce "hot spots" in the radar cross-section pattern of some turbojet aircraft, thus indicating there is a strong signal return from the ducts.
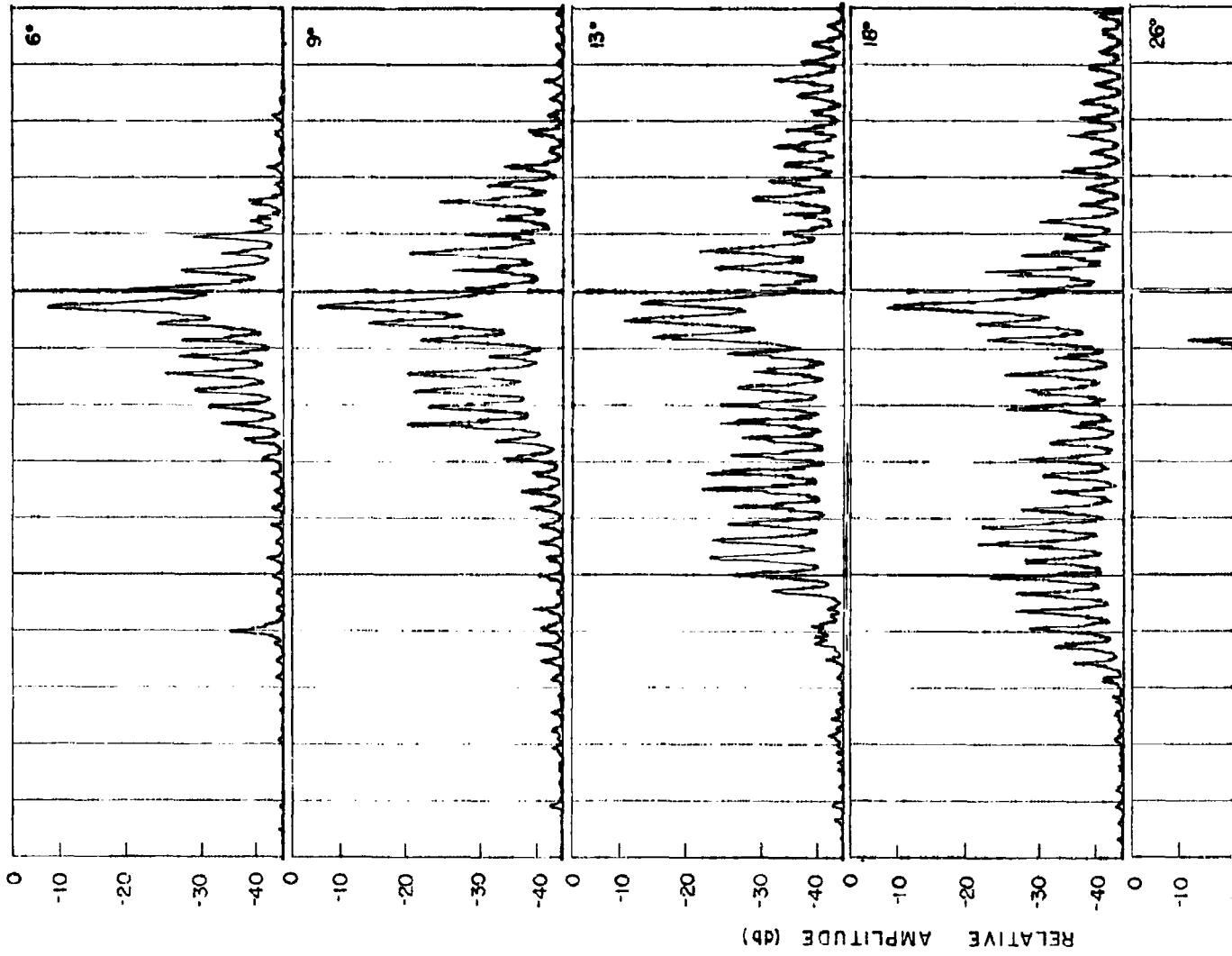
Figure 18 is the doppler spectrum of an approaching single-engine turbojet fighter aircraft. Note the 1200-cps modulation sidebands from the compressor. The lower frequency sideband (at 1200 cps) is 8.6 db below the airframe-line amplitude, while the upper sideband (at 3600 cps) is about 20 db lower.

Figure 19 is the doppler spectrum of a close formation of four approaching single-engine fighter aircraft of another type. All four aircraft were flying at the same velocity so that the airframe line shows up as a single line, but apparently their engine speeds were slightly different as they produced four distinct sidebands in the vicinity of 1500 cps at modulation frequencies around 2000 cps. There is an upper set of sidebands 2000 cps above the airframe line, but they do not appear within the range of this chart. Here again, the upper sidebands are 20 db weaker than the airframe line, while the lower sidebands are only from 1 to 5 db weaker.

In the very limited number of samples of turbojet aircraft available, the amplitude of the lower frequency compressor modulation sideband appearing in the doppler spectrum averaged only about 5 db below the airframe line, while the upper sideband was very much weaker. Also, in these samples only one predominant pair of sidebands appear in the spectrum.

Strong modulation from the compressors of most of the turbojet aircraft used as targets was detected at aspect angles relative to the nose up to at least 60°. However, no modulation due to the turbine stages has been detected thus far from the rear of a turbojet aircraft at S-band. This may be due partially to the fact that the turbine blades are usually somewhat smaller than a wavelength at S-band. Others have detected turbine modulation at X-band, however (4).
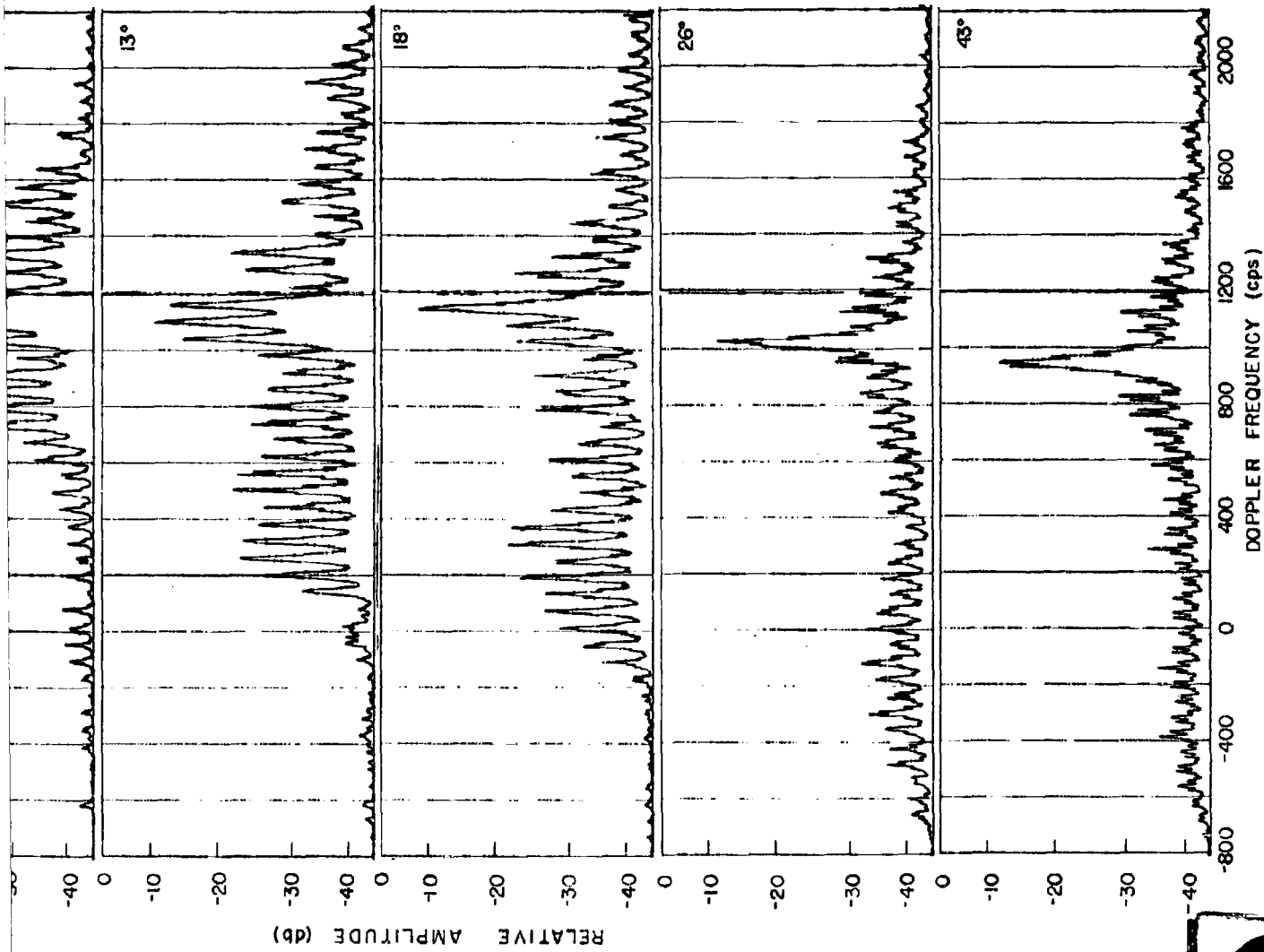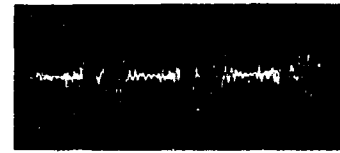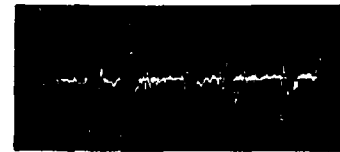
RELATIVE AMPLITUDE (db)

Fig. 16 - Doppler spectra of an approaching two-engine propeller-driven aircraft

(a)

Fig. 17 - Time-amplitude pictures of
the propeller doppler return of an
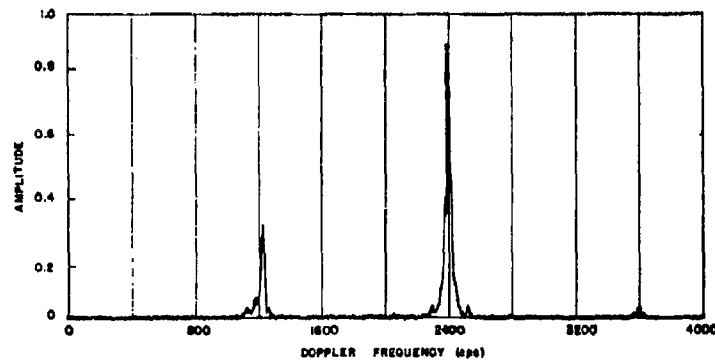approaching two-engine aircraft at
aspects of (a) 18° and (b) 26°

(b)

Fig. 18 - Doppler spectrum of an approaching
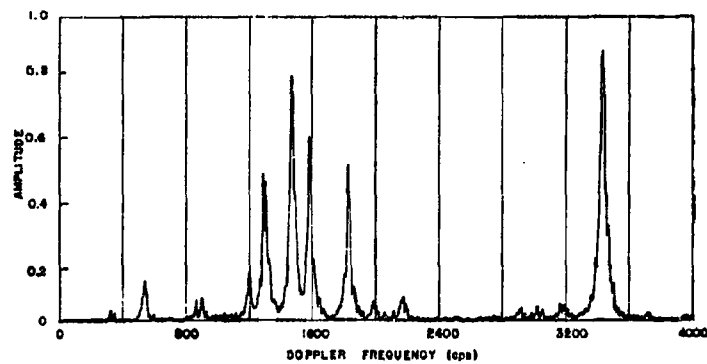single-engine turbojet aircraft

Fig. 19 - Doppler spectrum of four
single-engine turbojet aircraft

AIRFRAME DOPPLER SPECTRAL LINE

As stated in the introduction, the doppler return from the airframe will not be a single pure frequency, but will contain some velocity noise due to target scintillation. Thus, it would be expected that for a given sample time, the airframe line would appear to have some finite width when examined with a spectrum analyzer whose bandwidth was less than the frequency spread.

The width of the airframe line of a number of various types of aircraft targets was measured using the system shown in Fig. 20. The wideband doppler signal was fed into an automatic frequency tracking unit with an open-loop transfer function of $200/(300s+1)$ which translates a doppler frequency in the 100 to 6000 cps range to an i-f frequency of 50 kc, where the bandwidth is narrowed to 250 cps. The feedback path includes a limiter, frequency discriminator, integrator, and a voltage-controlled oscillator. The 50-kc i-f output of the tracker is translated back down to an audio frequency of about 300 cps and recorded on magnetic tape at 7.5 ips. A final frequency of 300 cps was selected in order to minimize the effect of tape recorder flutter, which is a constant percentage of the recorded frequency. A section of the tape was spliced into a 39-in. loop and played back at 7.5 ips into the analyzer, thus making the sample time 5.2 sec. Since the closed-loop time constant of the frequency tracking unit is 1.5 sec, any very slow variations in the target's velocity are tracked out, but any variations higher than about 0.4 cps are not appreciably affected. An analyzer bandwidth of 0.25 cps was used.
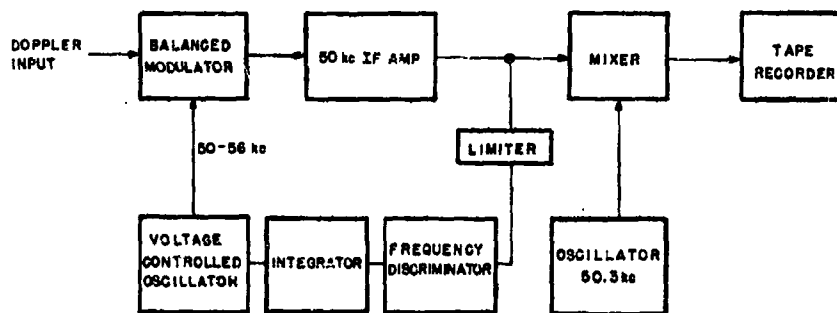

Fig. 20 - Automatic frequency tracking unit

A stationary target was first used to check the frequency resolution capability of the entire system. The radar, with its phase detector reference frequency offset, was locked on the Washington Monument, and a tape was made of the doppler output of the frequency tracker and mixer. (Offsetting permits tracking of a stationary target.) Figure 21 shows that the resulting width of the spectrum line was only about 0.7 cps, which includes any radar system instability, tape recorder flutter, and analyzer bandwidth.

Figure 22 is the spectrum of the airframe line of a DC-7 at an aspect of 135°. It can be seen that the half-power bandwidth, taking into account the system resolution, is approximately 7 cps. The average of the bandwidths of 10 samples of target similar in size and speed to the DC-7 was about 6 cps at aspects from 135° to 180° for a sample time of 5.2 sec. Figure 23 is the airframe line spectrum of a large multiengine turbojet traveling at a higher speed than the DC-7. The airframe line bandwidth here is about 15 cps. Figure 24 is the spectrum of a close formation of the same type turbojets at a tail aspect. It can be seen that there is a total spread of about 100 cps between the radial velocities of the
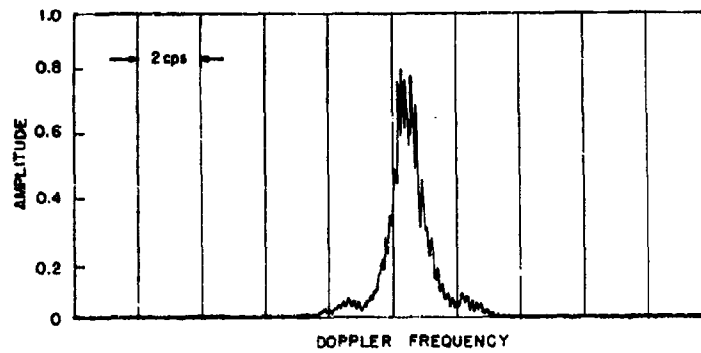
Fig. 21 - Doppler frequency spectrum of a fixed
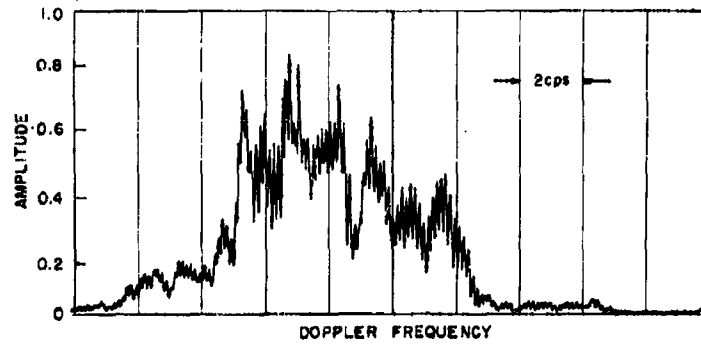target, indicating the system resolution

Fig. 22 - Airframe doppler frequency spectral
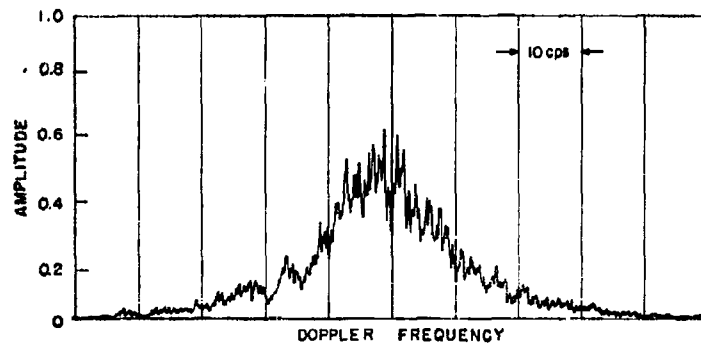line of a DC-7 at a 135° aspect

Fig. 23 - Airframe doppler frequency spectral line
of a large multiengine turbojet aircraft

individual aircraft within the formation in addition to the width due to scintillation. Figure 25 shows the spectrum of the formation for a short sampling time of 137 ms at two different times within the 5.2-sec period covered in the previous sample. Here the individual velocities of the aircraft are more clearly shown, and some of them appear to wander around within the 100-cps total spread. The method used to obtain the short samples is given in Appendix B.
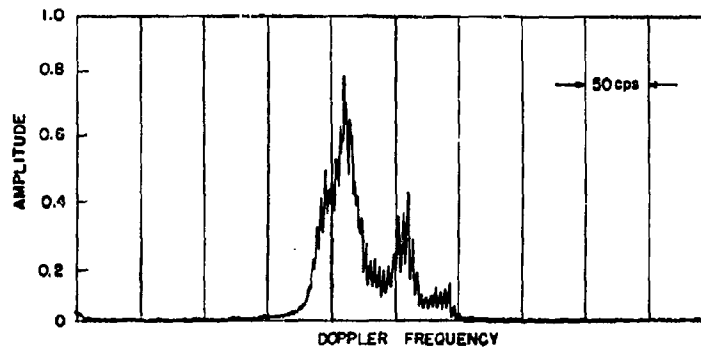
Fig. 24 - Airframe doppler frequency spectral line of
a formation of multiengine turbojet aircraft
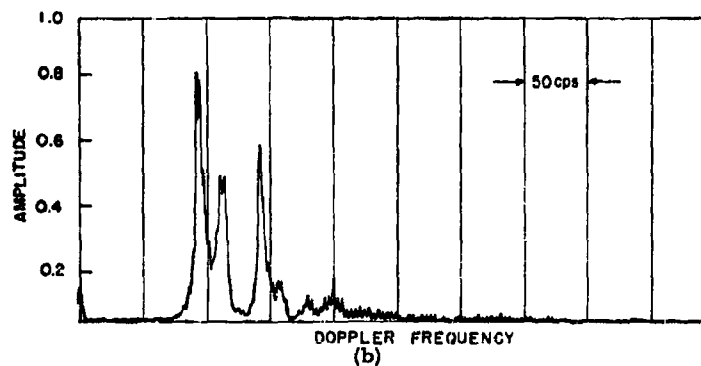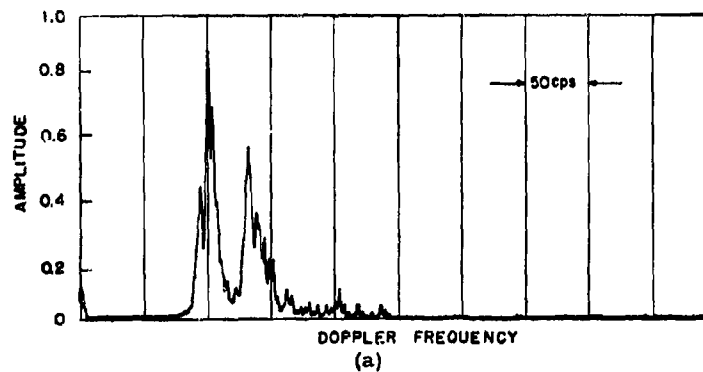
Fig. 25 - Airframe spectral lines for two 137-ms
sample times within the 5.2-sec sample of Fig. 24

There was not enough data taken to obtain any definite conclusion as to the correlation between type and aspects of aircraft targets and their airframe doppler line widths. It would be expected, however, that the results would depend also on aircraft velocity, type of maneuvering, and air turbulence.

VELOCITY NOISE SPECTRAL DENSITY

Range noise spectral power distribution of aircraft targets has previously been extensively investigated with pulse tracking radars (5). The results showed that most of the range noise power falls below 2 cps with noise components becoming insignificant above 10 cps. It might be expected that velocity noise would be related to the time derivative of the range noise. However, velocity information processing in a doppler radar is quite different from that of a pulse radar with, for example, a split-video range error detector, so that there is not necessarily a direct correlation between velocity noise measured with a doppler radar and that measured with a pulse tracking radar. Appendix C gives an example in which the two types of radars would give different results for a given situation.

The system used to measure the spectral density of the velocity noise is shown in Fig. 26. The output of the discriminator of the automatic frequency tracking unit shown in Fig. 20 is fed to a balanced modulator with a 250-cps carrier frequency. Thus, the frequency deviation of the signal from the long-time average doppler frequency is converted into amplitude modulation of a 250-cps carrier, in which form it can be recorded easily on magnetic tape. The modulated carrier is necessary because most of the noise components are of very low frequency and would be difficult to record directly. Since the time constant of the frequency tracking unit is 1.5 sec, the noise data is valid only for frequencies above about 0.4 cps. The modulated carrier is recorded at 1.5 ips on magnetic tape and then spliced into a 39-in. loop, giving a sample time of 26 sec. This allows about 10 cycles of 0.4-cps noise, giving a fair statistical sample at the lowest frequency of interest.
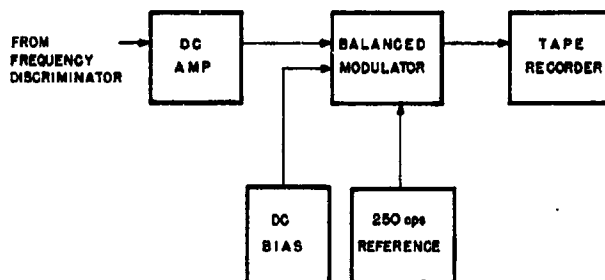

Fig. 26 - Block diagram of the system used to measure the spectral density of the velocity noise

The tape loop is played back continuously into a full-wave detector at 15 ips giving a frequency multiplication factor of 10. The demodulated signal is then analyzed on the LF-2aM spectrum analyzer using a noise bandwidth of 2.9 cps and a sweep range of 0 to 500 cps. The analyzer sweep rate, bandwidth, and output smoothing is such that the data is integrated for a full revolution of the tape loop. The 0 to 500 cps range of the analyzer output then actually represents 0 to 50 cps of real time noise data. The method used for calibration of the system is given in Appendix D.

Velocity noise measurements were made of a number of live targets of opportunity and several targets whose doppler had been previously recorded on tape. Figure 27 shows the noise spectral density out to 50 cps of three different propeller-driven commercial aircraft. The chart ordinates are in units of rms doppler frequency deviation at S-band per square root bandwidth, or rms cps/$\sqrt{cps}$. To change the units to knots/$\sqrt{cps}$, simply multiply the scale by the factor 0.1 knots/cps. The velocity noise power spectral density is proportional to the square of the amplitudes shown in the charts. In these samples, the highest values of noise density occur below 3 cps, the maximum being about 8 rms cps/$\sqrt{cps}$, while the value remains nearly constant at about 0.5 cps/$\sqrt{cps}$ between 10 and 50 cps. The slight rise beginning at 50 cps is part of the lower slope of a peak at the propeller modulation frequency. Even with 40 db of amplitude limiting and agc loops in the doppler amplifier and frequency tracker i-f amplifier, the discriminator is still very slightly amplitude sensitive. The extent of the contribution of amplitude noise to the values of velocity noise indicated on the charts was not fully determined, but it can be concluded, at least, that the actual values of velocity noise are no greater than the indicated values.

Figure 28 is the spectral density of the velocity noise of the same formation of large turbojet aircraft for which the airframe spectrum line was shown previously. As would be expected, the average value of noise density is much greater than that of smaller single aircraft, but the maximum value at very low frequencies does not appear to be appreciably greater.

In the statistically small number of aircraft targets investigated, there appear to be no distinctive peak in the velocity noise spectral energy distribution which might be characteristic of a particular type of aircraft. In general, however, the spectral density will be dependent somewhat upon target size, aspect, velocity, and maneuver. It may be that there is some correlation between doppler velocity noise and range noise spectral densities, but the matter was not sufficiently investigated to justify any definite conclusion. Much data already exists on range noise which, in turn, has been found to be related to angle noise (5).

CLUTTER

One of the merits of doppler radar is its ability to discriminate against clutter or stationary targets. However, some objects which are usually considered relatively stationary actually do have some motion which causes a portion of their doppler spectra to occur at other than zero frequency. Figure 29 is the spectrum of a tree-covered hillside on a windy day. The phase detector reference was offset to place zero doppler inside the system passband. The narrow peak at zero doppler frequency is due to the ground and other rigid objects included in the antenna beam and range gate which were not affected by the wind. It is seen that the remainder of the clutter doppler spectrum due only to the fluttering leaves and swaying branches resembles a Gaussian distribution with a standard deviation of about 7 cps.

Rain and clouds might be considered as other forms of clutter. However, useful information may be obtained regarding weather phenomena with doppler radar (6). Figure 30 is the doppler spectrum of a mass of dense rain clouds moving generally toward the radar at an elevation angle of 15°. The turbulance within the clouds is seen to spread the spectrum considerably. The main portion of the doppler return is centered at a relative velocity of about 20 knots. The smaller return which occurs between 35 and 40 knots may be due to the effect of wind shear within the pulse volume, which for this case is 290 yd in diameter by 164 yd in length.

(a)

(b)

(c)

FREQUENCY (cps)
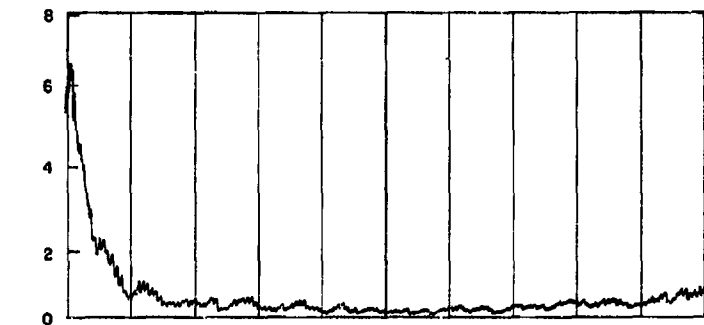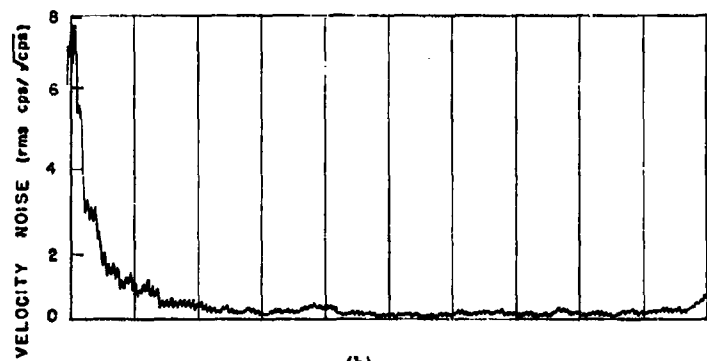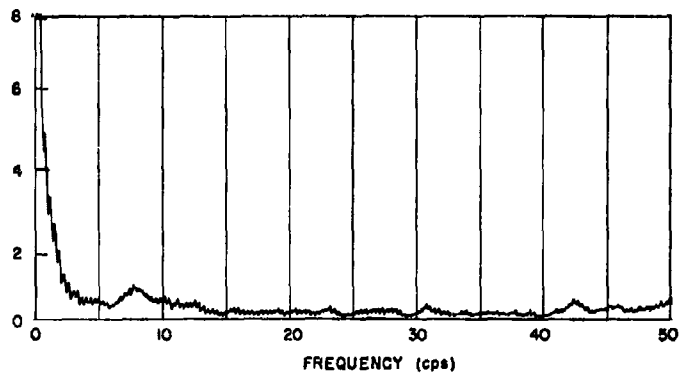
Fig. 27 - Doppler velocity noise spectral density of
(a) a DC-7 at 170° aspect, (b) Convair 340 at a 180°
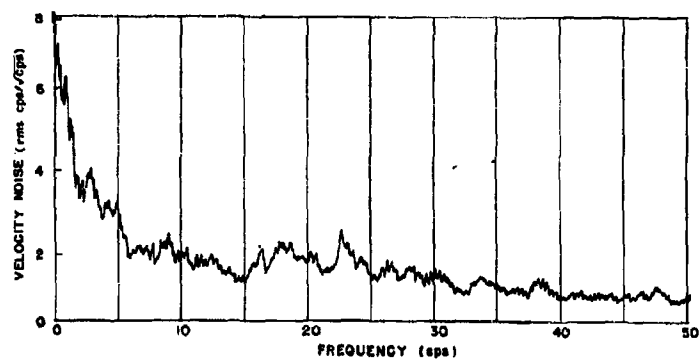aspect, and (c) a Lockheed Constellation at 170°
aspect

Fig. 28 - Doppler velocity noise spectral density of
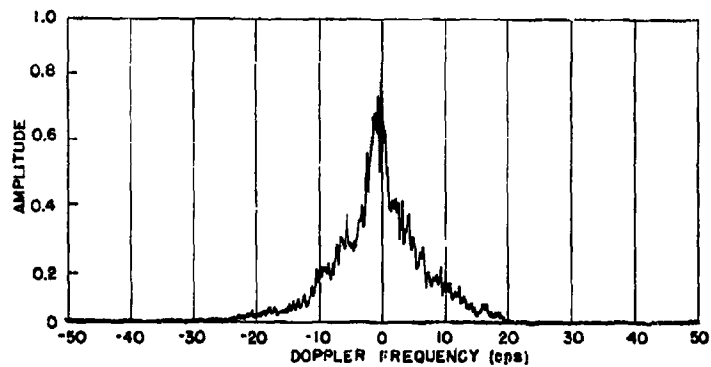a formation of turbojet aircraft at a 180° aspect

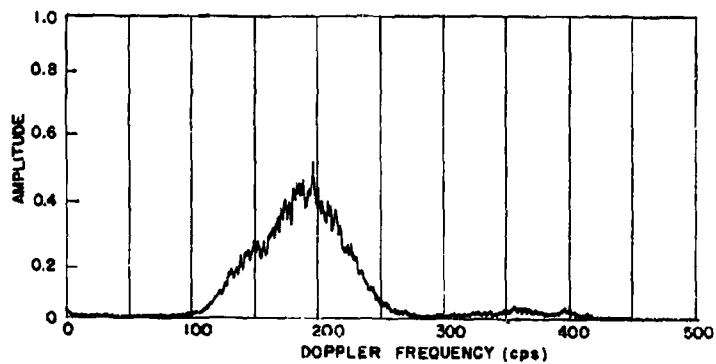Fig. 29 - Doppler spectrum of a tree-covered hillside

Fig. 30 - Doppler spectrum of rain clouds

DISCUSSION

Questions might arise as to the effects of these various complex spectra of aircraft targets on the tracking operation of doppler radars. For example, does a signal as seen by a coherent doppler radar contain as much energy as that seen by a noncoherent pulse radar. A previous investigation of this has shown that the coherence of radar echos from moving aircraft targets is excellent (7). This is evidenced by the fact that although a target's doppler spectrum quite often extends over a wide frequency range due to power plant modulation as seen in preceding examples in this report, the total power in these modulation spectral lines is usually small compared to that contained within a relatively small bandwidth centered around the airframe doppler spectral line. However, there is a practical limit to the minimum bandwidth which can be used in tracking the airframe spectral line and still utilize the major portion of the signal energy. This limit may range from a few cps for a small single aircraft to almost 100 cps for multiple large aircraft.

In order to compare the signal energies seen by doppler and pulse radars, a brief experiment was performed using a noncoherent channel added to the S-band pulse doppler radar at the 30-Mc i-f preamplifier output of the receiver. The noncoherent channel consisted of a conventional 30-Mc i-f amplifier, amplitude detector, and pulse stretcher. The agc voltage developed by the noncoherent video pulse stretcher was simultaneously compared to the agc voltage developed by the doppler amplifier in the 100 to 6000 cps band while tracking aircraft targets. The two channels were calibrated using a pure signal from a 30-Mc crystal oscillator. There appeared to be no significant difference between the signal strengths seen in the two channels, at least within the measurement accuracy of about 2 db of this relatively crude method.

When a system uses an automatic doppler frequency tracking unit, or speedgate, with a narrow bandwidth capable of resolving individual lines in the doppler spectrum, it is possible to accidentally lock on and velocity-track some of the modulation spectral lines instead of the airframe line. The ability of a speedgate to track the lower frequency compressor modulation sideband of a turbojet aircraft has actually been demonstrated. However, since the bandwidth of a practical speedgate usually will include at least two propeller modulation spectral lines it is not easy to track the propeller doppler return because the lines are often distributed over a wide frequency range in addition to their changing rapidly with target aspect angle. If the propeller spectral lines happen to be narrowly grouped and remain fairly constant with time, it is possible to roughly track them.

Some doppler radar systems do not fold the doppler spectrum about zero in a phase detector, but translate the spectrum down only to some moderate i-f frequency, such as 2 Mc, for example. The target doppler spectra for these systems will have the same characteristics as those given in this report in which the spectrum is folded, except that now zero doppler will fall at the 2-Mc i-f frequency much the same as if the phase detector reference frequency had been offset by 2 Mc in a folding system.

CONCLUSIONS

1. Rotating propeller blades produce doppler-shifted echos relative to the airframe due to radar energy reflected from the blades themselves. The major portion of the propeller doppler spectrum is always lower in frequency than the airframe line in a system which folds the spectrum about zero.

2. The return from the rear of a propeller consists mainly of periodic pulses of a doppler frequency proportional to the radial velocity of a discrete reflecting element on a blade. The reflecting element's radius on the propeller blade, hence its radial velocity, is a function of viewing aspect and is most clearly defined within limits determined by

the blade angles. Typically, these limits may be aspects between 15° and 30°. The resulting doppler spectrum roughly resembles a sin x/x type of amplitude distribution with the main lobe typically 600 cps wide and spectral lines spaced by the propeller blade modulation frequency.

3. The doppler return from the front of a propeller contains frequency modulation as well as amplitude modulation. At small aspect angles, the propeller doppler spectral lines are grouped in the vicinity of the airframe doppler frequency, while at larger aspects they become spread over a much greater portion of the spectrum below the airframe line. Again, the spectral lines are spaced by the propeller blade modulation frequency.

4. The doppler spectrum of an approaching turbojet aircraft contains modulation sidebands around the airframe line due to the rotating compressor blades. The first lower frequency sideband is the predominant one and, on the average, is only 5 db weaker than the airframe line. The amplitude of the higher frequency sideband is usually small enough to be considered insignificant. Compressor modulation can be detected at aspects up to at least 60°.

5. The airframe doppler spectral line has a finite width due to target scintillation. The width of the airframe line of aircraft such as the DC-7 was found to be about 6 cps, while that of a larger and faster aircraft was found to be as wide as 15 cps.

6. Measurements of velocity noise spectral density indicate that most of the noise energy lies below 3 cps.

REFERENCES

1. Holt, F.S., and Spencer, R.C., "Experimental Optical Investigation of Radar Backscattering," Air Force Cambridge Research Center Report AFCRC-TR-57-106, April 1957

2. Ridenour, L.N., editor, "Radar System Engineering," Radiation Laboratory Series, Vol. 1, New York:McGraw-Hill, 1947, p. 66

3. Kerr, D.E., editor, "Propagation of Short Radio Waves," Radiation Laboratory Series, Vol. 13, New York:McGraw-Hill, 1951, pp. 3-8, 445-469

4. "Flight Test Report on Feasibility Model, X-Band Pulse Doppler Airborne Interceptor Radar" (Confidential Report, Unclassified Title), Westinghouse Electric Corp., Air Arm Division, Contract AF 33 (616)-3700, May 15, 1959

5. Howard, D.D., and Lewis, B.L., "Tracking Radar External Range Noise Measurements and Analysis," NRL Report 4602, Aug. 31, 1955

6. "Doppler Radar Observations of Weather and Aircraft Spectra," Cornell Aeronautical Laboratory Report JA-1087-T-1, June 1957

7. Boyd, F.E., "The Coherence of Radar Echoes," NRL Report 4258 (Confidential Report, Unclassified Title), Dec. 8, 1953

APPENDIX A

FOURIER ANALYSIS OF A PULSE-PAIR TRAIN

Consider the waveform shown in Fig. A1. A Fourier analysis will show that

$$f(t) = A_{av} + \frac{2}{T} \sum_{n=1}^{\infty} \left[(\tau_2 + \tau_1) \frac{\sin \frac{n\omega(\tau_2 + \tau_1)}{2}}{\frac{n\omega(\tau_2 + \tau_1)}{2}} - (\tau_2 - \tau_1) \frac{\sin \frac{n\omega(\tau_2 - \tau_1)}{2}}{\frac{n\omega(\tau_2 - \tau_1)}{2}} \right] \cos n\omega t.$$

For example, if $\tau_2 = 2\tau_1$, and $\tau_1/T = 0.1$, the magnitude of the spectrum will appear as in Fig. A2(a).
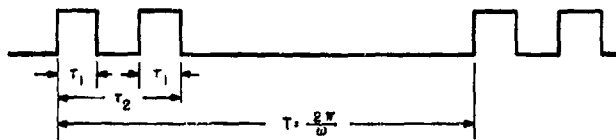
Fig. A1 - Waveform of a pulse-pair train

(a)

(b)
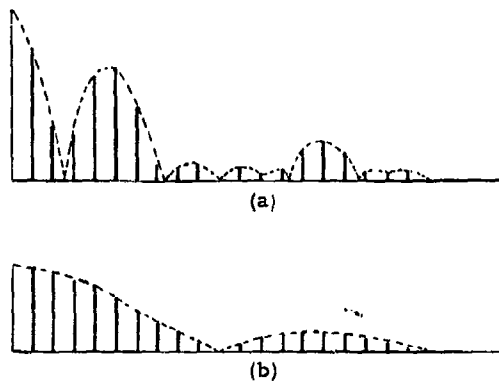
Fig. A2 - Pulse spectra of (a) pulse-pair train and (b) single-pulse train

29

For comparison, consider a single-pulse train with the same τ_1 and T as above. The Fourier analysis has the well-known sin x/x distribution:

$$f(t) = A_{av} + \frac{2\tau_1}{T} \sum_{n=1}^{\infty} \frac{\sin \frac{n\omega\tau_1}{2}}{\frac{n\omega\tau_1}{2}} \cos n\omega t.$$

The spectrum of this is shown in Fig. A2(b).

APPENDIX B

METHOD OF OBTAINING SHORT SAMPLES FOR ANALYSIS

A regenerative process utilizing an Ampex Model 401A Tape Recorder was used to obtain 137-ms samples of data. This process takes a short segment of data and regenerates it, placing the regenerated segments end to end on magnetic tape to make a continuous recording so that it can be analyzed using the conventional tape loop playback method. A block diagram of the system is shown in Fig. B1. With S open, the 401A records normally. When S is closed, the low output impedance of the cathode follower (C.F.) essentially grounds out the input signal and simultaneously applies the feedback signal to the record input with no dead time. Since the spacing between the record and playback heads in the 401A is 2.06 in., at 15 ips the time required for a recorded signal to reach the playback head is 137 ms. This recorded signal is then reapplied through the feedback loop to the record head, and the process is repeated every 137 ms. This process is continued to at least 2.6 sec so that a 39-in. section of tape is obtained to splice into a loop for analyzing.
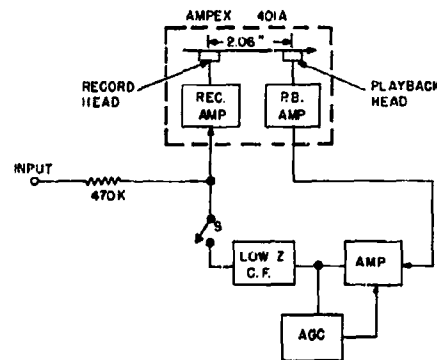
Fig. B1 - System for making
short data samples

An automatic gain controlled amplifier is used in the feedback path to help keep the record level constant. The amplifier is not absolutely necessary, but without it the gain setting is very critical. If the gain is not set exactly, the record level will either rise to saturation or exponentially diminish, depending whether the setting was too high or too low. Some equalization may be necessary to keep the signal-to-noise ratio at a reasonable level as the tape noise accumulates each cycle of regeneration.

31

APPENDIX C

A COMPARISON OF VELOCITY NOISE PHENOMENA OF A PULSE TRACKING RADAR AND A DOPPLER RADAR

As an example of a configuration in which a pulse radar and a doppler radar would indicate different velocity noise spectral distributions, consider two small equal reflecting areas connected by a nonreflecting rod of length $\Delta R = R_2 - R_1$ as shown in Fig. C1. Assume that as the reflectors rotate about the rod midpoint through a small angle $\Delta \theta$ from position A to position B, the sum of the magnitudes of the signals returned remain constant, but that at position A the signal return is predominately from the area at range R_1, and at position B it is predominately from the area at R_2. Assume also that R_1 and R_2 remain essentially constant as the system rotates from A to B. An analog of this configuration could exist conceivably on an aircraft where the reflecting areas could be radar cross section "hot spots" on the airframe. For this example, let ΔR be an integral number of wavelengths so that the return from R_2 will be in phase with the return from R_1.
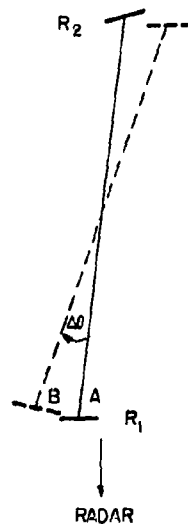
Fig. C1 - Assumed reflecting area configuration

In the case of a pulse radar with a split-video range error detector, if the range error is zero in position A, and then the reflectors rotate to position B, a range error voltage will be developed as shown in Fig. C2(a), provided that ΔR is less than one-half

32

(a)
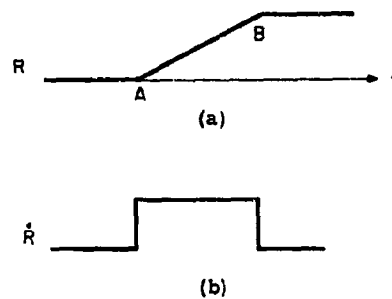
Fig. C2 - Response of a pulse
radar: (a) range e r r o r; (b)
range rate developed from a
split-video range error detector

(b)

a pulse length. The apparent velocity, being the time derivative of range, will have the
form shown in Fig. C2(b). However, in a doppler radar where velocity is derived from
the doppler frequency or time rate of change of phase, there will be no apparent velocity
developed in this example because there will be no net change in phase.

APPENDIX D

CALIBRATION OF VELOCITY NOISE SPECTRAL DENSITY

A square wave of frequency modulation of known deviation was used in calibrating the velocity noise measuring system for each data run. For example, a 10-cps peak-to-peak frequency deviation of any carrier frequency within the doppler band at a modulation frequency of 1 cps will result in a spectral distribution similar to that in Fig. D1. This can be done at audio frequencies and fed directly into the frequency tracking unit. Since the ratio of the peak-to-peak to rms deviation of the square wave first harmonic is 2.3, a scale factor can be obtained from

$$S = \frac{\Delta f_{p-p}}{2.3 \times A}$$

where A is the amplitude of the first harmonic, or fundamental, line in scale divisions on the calibration recording. For the example in Fig. D1, the scale factor would be

$$S = \frac{10}{2.3 \times 0.57} = 7.6 \text{ rms cps/div.}$$
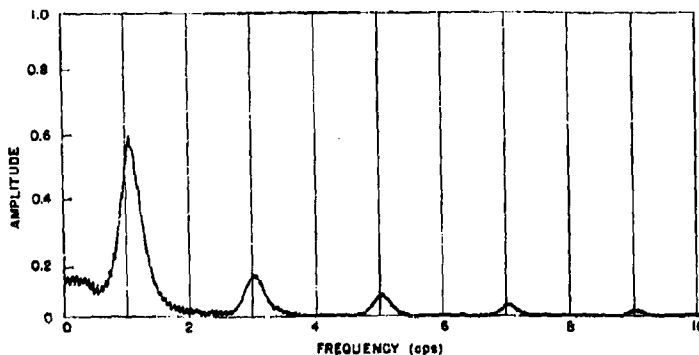
Fig. D1 - Spectral density square wave calibration recording

The noise power in a given region is proportional to the bandwidth. Since the LF-2aM spectrum analyzer measures voltage, the analyzer output amplitude when measuring noise will be proportional to the square root of the analyzer bandwidth. However, a frequency multiplication factor of 10 was used for these velocity noise measurements, so that the effective bandwidth at the true noise frequency is 1/10 the analyzer bandwidth. At an analyzer noise bandwidth of 2.9 cps, the noise calibration factor in this example is

$$N = \frac{7.6 \text{ rms cps/div}}{\sqrt{0.29 \text{ cps}}} = 14.1 \text{ rms cps/}\sqrt{\text{cps}}\text{/div.}$$

34